I&EC research
Industrial & Engineering Chemistry Research

Research Note

pubs.acs.org/IECR

Spatial Profiles in RuO_2–CuO–NaCl/SiO_2 Packed-Bed Propylene Epoxidation Reactors

Bahman Zohour,[†] Daniel Noon,[†] Anusorn Seubsai,[‡] and Selim Senkan*[,†]

[†]Department of Chemical Engineering, University of California, Los Angeles, California 90095, United States
[‡]Department of Chemical Engineering, Kasetsart University, Bangkok, Thailand 10900

ABSTRACT: The spatially resolved species concentration and temperature profiles in a catalytic fixed-bed propylene epoxidation reactor were determined for RuO_2–CuO–NaCl/SiO_2 catalysts, using microprobe sampling and online gas chromatography. Experiments were performed at furnace temperatures of 250 and 270 °C and feed gas compositions of 1 mol % C_3H_6, 4 mol % O_2, and $1^2/_3$ mol % C_3H_6, $3^1/_3$ mol % O_2, both with 95 mol % He dilution. The pressure was atmospheric, and the gas hourly space velocity (GHSV) was ~30 000 h^{-1}. The spatial profiles indicated that propylene oxide (PO) and acetone production exhibited well-defined induction periods. In contrast, acrolein (AC) formation was prompt and occurred early in the catalyst bed. These findings point to two different mechanisms associated with the formation of PO/AT and AC, respectively. The absence of any measurable propanal in the product mix suggests that C2 oxametallacycle propylene (C2OMMP) may be the preferred route for PO formation in this catalytic system. The spatial profiles reported represent information-rich data that are of significant utility for the development and validation of detailed chemical kinetic mechanisms for propylene partial oxidation in general and epoxidation in particular.

INTRODUCTION

Propylene oxide (PO) is an important intermediate for the production of a large variety of valuable consumer products such as polyurethane foams, propylene glycol, cosmetics, food emulsifiers, fumigants, and insecticides.[1,2] Over eight million tons of PO are produced annually, mostly via the chlorohydrin and peroxidation processes.[1,2] Recently, a process using H_2O_2 has also been commercialized.[1,3] However, the direct synthesis of PO from propylene and oxygen remains an important goal in industrial catalysis. The technology, the economics, and the environmental impacts of current as well as alternate propylene epoxidation processes were reviewed by Cavani and Teles in 2009[1] and Nijhuis et al. in 2006.[2]

The direct epoxidation of propylene by oxygen involves the following overall stoichiometry:

$$C_3H_6 + \frac{1}{2}O_2 \rightarrow C_3H_6O$$

However, besides PO, the partial oxidation of propylene can also form a variety of byproducts, such as acetone (AT), acrolein (AC), propionaldehyde (propanal, PA), acetaldehyde (AA), and formaldehyde (FA), together with deep oxidation products of CO and CO_2. Earlier research on direct PO formation involved the use of Ag-based catalysts in an attempt to produce the commercial success of ethylene oxide (EO) production.[1,2,4] Many other catalytic materials and techniques were also explored for PO synthesis, including silica-supported Cu,[5] various single and mixed metal oxides,[6,7] Au-based catalysts with H_2[8] or H_2O[9] as co-reactants, titania-based catalysts,[10] and molten salts of metal nitrates,[2] in addition to the use of O_3[11] and nitrous oxide[2] as reactants. PO synthesis by Ag_3 clusters deposited on thin alumina films prepared via molecular beam techniques was also performed.[12] Recently, we reported the discovery of a new class of silica-supported multimetallic RuO_2–CuO–NaCl catalysts for the direct epoxidation of propylene by O_2 under atmospheric pressure.[13] This trimetallic catalyst, prepared via co-impregnation, exhibits PO selectivities of 40%–50% with propylene conversions of 10%–20% at 240–270 °C and 1 atm.[13] It is important to note that all the aforementioned prior research involved measurements of reactor exit conditions, which provide data of limited information content.

PO is believed to occur via the formation of an oxametallacycle propylene intermediate (OMMP, where M represents a general surface metal atom) similar to that proposed for ethylene epoxidation.[14,15] However, the presence of the methyl group in propylene results in the formation of two distinct OMMP structures, which lead to different products. For example, C1-OMMP formation (i.e., surface O is bonded to the $=CH_2$) can directly form PO by cyclization and, via C1 to C2 H atom transfer, PA. Similarly, C2-OMMP formation (i.e., surface O is bonded to the $=CHCH_3$) can also produce PO and, via C2 to C1 H atom transfer, AT. These OMMP structures and plausible subsequent reactions are shown below:

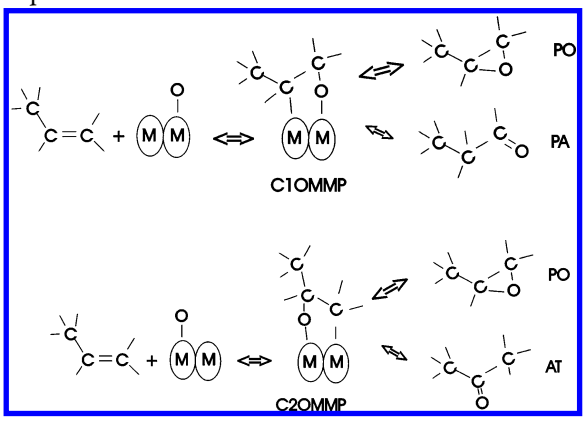

Received: July 26, 2013
Revised: February 27, 2014
Accepted: March 19, 2014
Published: March 19, 2014

dx.doi.org/10.1021/ie402416s | *Ind. Eng. Chem. Res.* 2014, 53, 6243–6248

Based on this representation, the relative amounts of PA and AT produced can indicate the dominant OMMP structure expected to be present in a given catalytic system. On the other hand, the formation of AC requires O insertion into the methyl group (C3) of propylene, which is an entirely different pathway, and, as such, could involve a different surface metal atom M.

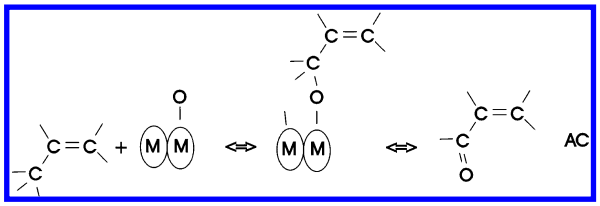

It should be recognized that the products PO, AT, and PA can also undergo subsequent isomerizations and related reactions.[16] Similarly, the formation of CH_3CHO and HCHO could be taken into account by the formation of a C1OMMOC2 structure, as shown below:

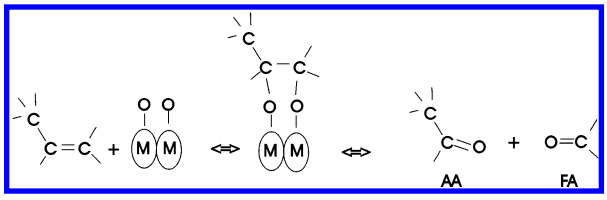

Propylene, as well as all partial oxidation products, can undergo further oxidations, ultimately forming CO_2 and H_2O.

As evident from the above discussion, propylene partial oxidation involves a highly complex network of parallel and sequential reactions. Consequently, to better control and optimize the propylene epoxidation reaction, detailed chemical kinetic mechanisms (DCKM) of the underlying surface reactions (as well as possible gas-phase reactions) must be developed *and* validated over a broad range of conditions. DCKM comprise a comprehensive description of chemical transformations in terms of *irreducible* chemical events or *elementary reactions* for which independent rate coefficient parameters, frequently expressed in the form $k = AT^n \exp[-E/(RT)]$, are either available from direct measurements or estimated from theoretical considerations.[17] DCKM are then combined with transport models for the simulation and optimization of propylene partial oxidation reactors.[17] However, the validation of DCKM require experimental data of high information content, because of the presence of a large number of species participating in an even larger number of elementary reactions.[17] In this regard, reproducing only the reactor exit concentrations will not be a particularly demanding test for mechanism validation. On the other hand, the prediction of the absolute *concentration profiles*, i.e., shapes, of all the major and minor species within the catalytic packed beds represents a more rigorous test for DCKM validation. It can be argued that traditional experiments in which reactor exit measurements at different gas flow rates and/or catalyst loadings are performed can be used to obtain similar data. However, traditional approaches rapidly become very tedious and extremely time-consuming especially when data of high information content are needed. Consequently, the development and use of new experimental techniques that allow for the rapid acquisition of spatial profiles in reactors is desirable. In an earlier study, Wong et al.[18] proposed a DCKM for the catalytic partial oxidation of propylene to AC and acrylic acid, together with the formation of numerous byproducts. Although these authors did not explicitly consider PO formation pathways in their mechanism, their work represents a good starting point for the development of DCKM for propylene epoxidation.

Here, we report, for the first time, the spatially resolved species concentration and temperature profiles in a catalytic fixed-bed propylene epoxidation reactor using microprobe sampling for the RuO_2−CuO−NaCl/SiO_2 catalyst discovered recently in our laboratories.[13] Although microprobe sampling techniques have long been used in high-temperature flame combustion research to obtain spatial temperature and concentration profiles,[19] their adaptation to and use in heterogeneous catalysis is relatively recent. Earlier applications of microprobe sampling to catalysis include the catalytic partial oxidation (CPO) of methane producing CO and H_2[20] and the oxidative coupling of methane (OCM) to form C_2H_6 and C_2H_4.[21]

EXPERIMENTAL SECTION

Experiments were performed using a fixed-bed tubular reactor system, as shown in Figure 1. The silica-supported multimetallic

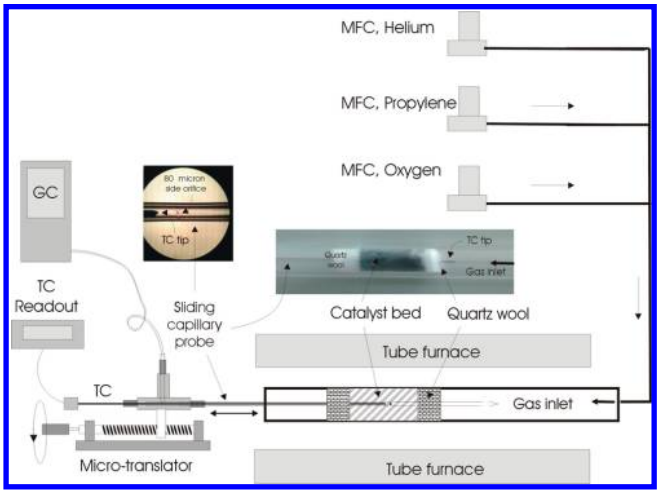

Figure 1. Schematic of the mass flow control system, heated quartz tube reactor setup, capillary sampling probe and gas chromatography, and temperature measurement system. Photographic images of the packed-bed reactor, magnified capillary probe, 80 μm sampling orifice, and inserted thermocouple are also shown.

RuO_2−CuO−NaCl catalyst was prepared via the *co-impregnation* method described previously.[13] Briefly, predetermined weights of amorphous fumed silica powder (SiO_2, Alfa Aesar, surface area of 145 m^2/g, bulk density of powder ≈ 0.2 g/cm^3) were mixed with an aqueous solution of ruthenium [$(NH_4)_2RuCl_6$, Aldrich], copper [$Cu(NO_3)_2$, Alfa Aesar, ACS, 98.0%−102.0%], and sodium [NaCl, Alfa Aesar, 99.99% (metals basis)]. The metal salt solution was then allowed to impregnate the support for 24 h in air. The resulting material was then heated at 165 °C until dried, and calcined at 480 °C for 6 h in air. The catalyst used in the experiments had a Ru:Cu:Na metal ratio of 4:2:1 (weight ratio, or ∼3:4:4 atomic ratio) at 12.5 wt % total metal loading maximized the PO selectivity.[22] Fifty milligrams (50 mg) of this catalyst was packed into a 6-mm-diameter quartz tube and sandwiched between two quartz wool plugs, each weighing 10 mg (Figure 1). The bulk density and void fraction of the bed were determined to be about 0.27 g/cm^3 and 0.90, respectively, assuming nonporous SiO_2 nanoparticles having a solid density of 2.65 g/cm^3. The reactor was placed inside a cylindrical tubular furnace, which also preheated the feed gases. Using electronic mass flow controllers (MFC, MKS Billerica, MA), the total flow

dx.doi.org/10.1021/ie402416s | *Ind. Eng. Chem. Res.* 2014, 53, 6243−6248

of reactant gases was maintained at 100 cm^3/min at STP in all of the experiments.

Gas sampling was accomplished by centrally inserting a conically tapered and closed-end quartz capillary tube (800 μm, Friedrick and Dimock, Millville, NJ) into the packed bed, followed by gas analysis using online gas chromatography (Varian 4900 mini GC, with molecular sieve 5A and PoraPLOT U columns). The capillary had several 80-μm-diameter orifices laser-drilled on its side to withdraw gases from within the bed (see inset in Figure 1). The location of the sampling orifice and the overall length of the probe were designed such that the capillary tip always remained well outside the packed bed at any sampling position to avoid channeling and gas bypass. That is, the probe body always remained inserted into the entire bed length, including the quartz wool plugs. If the probe tip were moved into the bed during measurements, channeling would occur through the hole created. The capillary probe withdrew gas samples at a rate of ~5 cm^3/min at STP, thus minimally perturbing the gas flow within the reactor, which was flowing at a rate of 100 cm^3/min at STP. At this sampling rate, the residence time of the gases in the capillary probe can be estimated to be in the range of 25−50 ms. Temperature measurements were performed by placing a thin (250-μm-diameter) K-type thermocouple inside the capillary probe in the absence of gas withdrawal. The tip of the thermocouple was positioned at the sampling orifice. Temperature and concentration profiles were obtained by moving the capillary (with and without the thermocouple) in the axial direction using a micropositioning device (Velmex, Bloomfield, NY). Positional accuracy associated with the placement of the capillary probe within the reactor is estimated to be ±0.25 mm. Similar uncertainty also would be expected to exist between the temperature and concentration profiles.

The experiments were carried out at two distinct furnace temperatures of 250 and 270 °C under a pressure of 1 atm and at a gas hourly space velocity (GHSV) of ~30 000 h^{-1}. Two feed gas compositions were explored: 1 mol % C_3H_6 (Matheson, 99%), 4 mol % O_2 (Matheson, 99.9%), and 95 mol % He (Matheson 99.99%); and $1^2/_3$ mol % C_3H_6, $3^1/_3$ mol % O_2 and 95 mol % He. These feed streams correspond to O_2/C_3H_6 ratios of 4 and 2, respectively.

The propylene conversions and product selectivities were calculated on the basis of carbon atom balances. GC calibrations for propylene, oxygen, and CO_2 were performed using mass flow controllers (MKS) and He as a carrier gas. Calibrations for PO, AC, AT, and PA were performed by vaporizing known quantities of the liquid in a heated, evacuated 2250 cm^3 stainless steel tank and using He as a carrier gas.[13] All calibrations yielded linear five-point curves with a correlation factor of at least $R^2 = 0.995$, using the peak area as the basis for GC calculations.

RESULTS AND DISCUSSION

Before presenting the results, several properties of the RuO_2−CuO−NaCl/SiO_2 catalyst should be noted. First, this catalyst is well-documented to require ~1 h of activation;[13] consequently, the results reported here were obtained after this period. Second, this catalyst is also known to exhibit deactivation after 6 h of continuous operation, because of the loss of chlorine.[13] Although co-feeding chlorinated hydrocarbons at a parts per million level remedies this problem,[22] we did not implement this method. Instead, experiments were performed during the initial 2−5 h age period of the catalysts, after which the catalysts were replaced.

In Figures 2 and 3, the spatially resolved temperature and species mole percent profiles are presented for the feed O_2/C_3H_6 ratio of 2 at furnace temperatures of 250 and 270 °C, respectively. A total of seven species were quantified: O_2, C_3H_6, PO, AT, AC, H_2O, and CO_2. Concentrations of other likely products (e.g., PA and AA) were too low for detection using the GC system with any appreciable accuracy. With the exception of the H_2O concentrations, which were calculated from oxygen atom balances, all the species were quantified directly from GC measurements, using a multipoint GC calibration process performed before the experiments. In Figures 4 and 5, the corresponding spatial profiles for the PO and CO_2 selectivities and C_3H_6 conversions are presented.

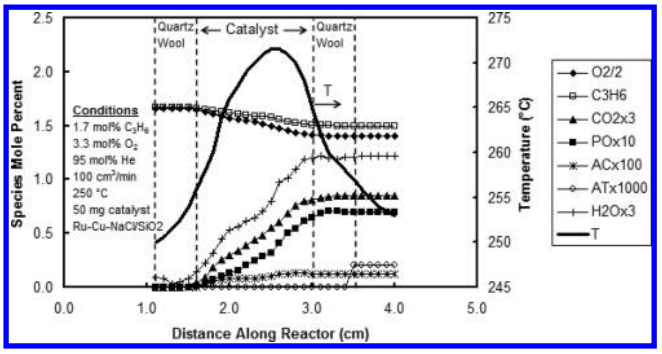

Figure 2. Species concentration profiles, including O_2, propylene (C_3H_6), CO_2, propylene oxide (PO), acrolein (AC), acetone (AT), and H_2O and temperature profile for a feed of $1^2/_3$ mol % C_3H_6, $3^1/_3$ mol % O_2, and 95 mol % He at 250 °C.

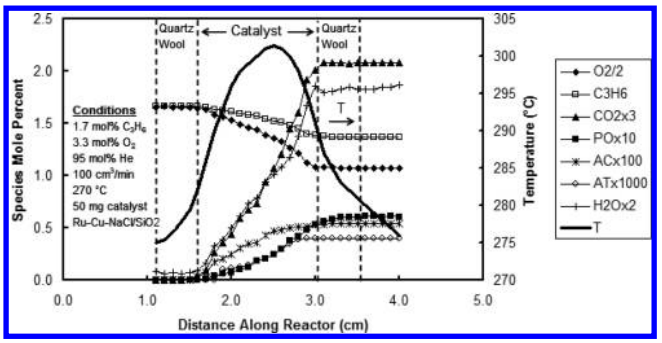

Figure 3. Species concentration profiles, including O_2, propylene (C_3H_6), CO_2, propylene oxide (PO), acrolein (AC), acetone (AT) and H_2O and temperature profile for a feed of $1^2/_3$ mol % C_3H_6, $3^1/_3$ mol % O_2, and 95 mol % He at 270 °C.

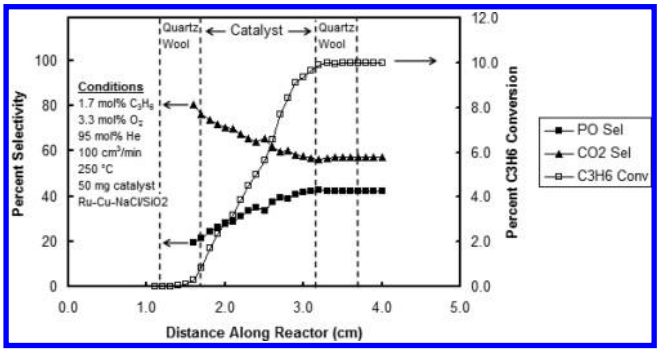

Figure 4. Propylene oxide (PO) selectivity, CO_2 selectivity, and propylene (C_3H_6) conversion profiles for a feed of $1^2/_3$ mol % C_3H_6, $3^1/_3$ mol % O_2, and 95 mol % He at 250 °C.

In all the figures, the positions of the catalyst bed and quartz wool packing are indicated by vertical dashed lines; the catalyst

dx.doi.org/10.1021/ie402416s | Ind. Eng. Chem. Res. 2014, 53, 6243−6248

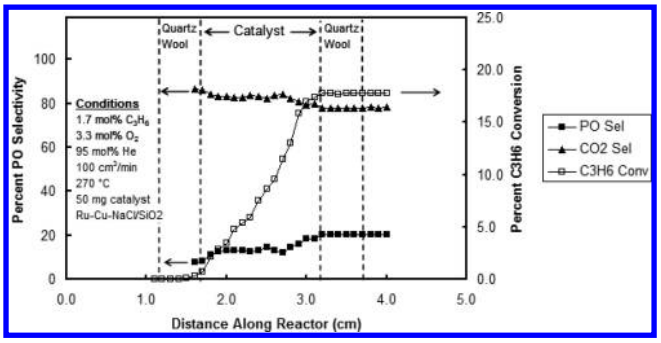

Figure 5. Propylene oxide (PO) selectivity, CO_2 selectivity, and propylene (C_3H_6) conversion profiles for a feed of $1^2/_3$ mol % C_3H_6, $3^1/_3$ mol % O_2, and 95 mol % He at 270 °C.

packing starts at ~1.5 cm and ends at ~3.0 cm, corresponding to a bed depth of 1.5 cm. As evident from Figures 2 and 3, the spatial concentration and temperature profiles measured within the bed provide information-rich data on the kinetics and mechanism of the propylene and oxygen reaction. In contrast, the profiles at the catalyst exit were essentially featureless and contain very limited information.

As seen in Figure 2, the temperature increased to a maximum of ~272 °C at 1.1 cm into the catalyst bed (i.e., at a distance of 2.6 cm along the reactor), corresponding to a temperature rise of ~22 °C, then decreased toward the exit of the reactor. Since the reactor was not adiabatic, this temperature profile is expected for an exothermic reaction. The possible presence of radial temperature gradients was also explored by placing multiple thermocouples at different radial positions at the same axial position. These studies indicated radial temperature differences that were within measurement errors of 2−5 °C, which suggests that the treatment of the reactor as being quasi one-dimensional appears to be a reasonable assumption. The temperature decreases observed in the later stages of the catalytic bed are indicative of the increased importance of product adsorption on the title reaction. As product concentrations increase in the gas phase, their desorption rates from the catalyst surface should decrease, thereby decreasing the overall rate of the reaction. Consequently, decreases in the heat generation rate can no longer exceed heat losses into the furnace (at 250 °C), resulting in a net decrease in reactor temperature at increased propylene conversions.

An important issue that must also be considered in the acquisition of accurate temperature profiles in reactors is the thermal conduction along the thermocouple wires. Conduction can result in temperature smoothing and profile shifts, especially when large temperature gradients (e.g., >100s °C/mm, as seen in flames) exist.[19] However, in the current experiments, such effects appear to be relatively insignificant.

The species profiles shown in Figure 2 at a feed temperature of 250 °C show both confirmatory and new features. First, the integral (i.e., exit) reactor performance was ~10% C_3H_6 conversion and 42% PO and 58% CO_2 selectivities, consistent with the O_2/C_3H_6 ratio of 2 (see also Figure 4) and previous experiments.[13] Second, the quartz wool packing had no catalytic activity, with respect to either propylene or the products, as all the concentration profiles remained flat prior to and after the catalyst bed. Third, reactions outside the catalyst bed can also be ruled out under the prevailing conditions. The fact that the measured concentration profiles remained flat (i.e., did not change with axial position within the quartz wool and reactor exit) supports the notion that reactions inside the sampling capillary were unimportant in our experiments. Fourth, the entire catalyst bed depth was actively utilized in creating the integral results (i.e., PO levels monotonically increased with distance along the reactor until the end of the catalyst bed). Finally, there was a sudden increase in the AT concentration at 3.4 mm (i.e., within the quartz wool packing), which can be attributed to the detection limits of the GC. Evidently, at the lower temperatures associated with the downstream quartz wool section and beyond, the increased gas density was sufficient to bring AT levels above the detection limits of the GC.

From Figure 2, it can be seen that PO formation started early in the catalytic bed and steadily increased with distance along the reactor, reaching a peak level of ~0.075%. On the other hand, CO_2 formation rate was faster, ultimately reaching a peak level of 0.25% at the exit, concomitant with the formation of H_2O (peaking at 0.38%). The higher CO_2 formation rate is not surprising,since 3 moles of CO_2 are produced per mole of C_3 species combusted. The profiles presented in Figure 4 reveal that PO selectivity also steadily increased and that for CO_2 decreased with increasing residence time in the reactor. These results clearly present useful trends that can be exploited for the design and operation of packed-bed reactors to improve PO selectivities. For example, increasing residence time can be beneficial in improving PO selectivity under the prevailing conditions.

The corresponding spatial profiles along the reactor at 270 °C feed temperature are shown in Figure 3. In this case, the temperature peak of 301 °C occurred at a distance of 2.6 cm along the reactor (i.e., 1.1 cm within the catalyst bed). Under these conditions, propylene conversion expectedly increased to a value of ~17.5%, as shown in Figure 5. This increase corresponds to an apparent activation energy of ~11 kcal/mol. However, the higher feed temperature of 270 °C had a significant detrimental effect on PO formation, both with respect to concentration (Figure 3) and selectivity (Figure 5). For example, the peak PO levels were only 0.06%, while CO_2 levels increased to 0.65%. The apparent activation energy for CO_2 formation corresponds to ~15 kcal/mol. Similarly, the PO selectivity only reached 20% (Figure 5), in contrast to 80% for CO_2. At 270 °C, the spatial profile for PO selectivity also exhibited a weak increasing trend, with respect to the distance along the reactor, in marked contrast with the results at 250 °C (Figure 4).

As noted earlier, trace levels of AC and AT were also produced in the current experiments, the profiles of which are shown in Figures 2 and 3. AC clearly was more abundant than AT under the conditions investigated. The absence of any measurable PA in the product mix may suggest that C2OMMP is the major route for PO formation, which also produces AT. However, the subsequent destruction of PA cannot be ruled out without a detailed chemical kinetic analysis. At a feed temperature of 250 °C (Figure 2), the peak levels of AT and AC were ~0.2×10^{-3} % and ~0.1×10^{-2} %, respectively. That is, AC levels were a factor of ~5 higher. It is interesting to note an abrupt increase in AT levels at the exit of the catalyst bed in Figure 2. This is related to the insensitivity of the GC to the low concentrations of AT early in the reactor. That is, sampling probe artifacts can be ruled out, since at slightly higher concentrations (i.e., at 270 °C, Figure 3), AT profiles exhibit the expected trends. Unlike PO, increasing the feed temperature to 270 °C increased the AT and AC peak levels to 0.4×10^{-3} % and 0.5×10^{-2} %, respectively (see Figure 3). Concentrations reported on Figures 2 and 3 suggest apparent activation energies of ~11 and ~30 kcal/mol for AT and AC formation reactions, respectively. The higher-temperature sensitivity of AC formation is also consistent with the relatively weaker allylic C−H bonds.

dx.doi.org/10.1021/ie402416s | *Ind. Eng. Chem. Res.* 2014, 53, 6243−6248

In addition to their magnitudes, the shapes of the concentration profiles presented in Figure 3 also provide new insights on the kinetics and mechanisms of formation of AC, AT, and PO. For example, AC formation can be seen to be prompt, exhibiting its highest rate at the entrance to the catalytic bed. In contrast, AT and PO exhibited a well-defined induction period. These results are consistent with the two different mechanisms associated with the formation of AC and PO/AT, respectively, as discussed earlier.

In order to quantify the effects of feed gas composition on species concentration profiles, experiments were also performed at the O_2/C_3H_6 ratio of 4 and at a feed temperature of 250 °C, and these results are presented in Figure 6. The corresponding

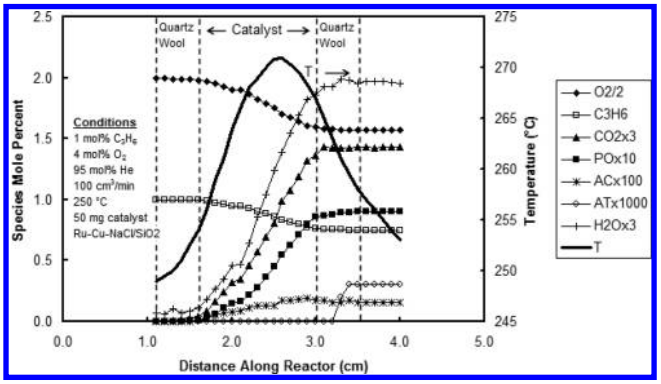

Figure 6. Species concentration profiles, including O_2, propylene (C_3H_6), CO_2, propylene oxide (PO), acrolein (AC), acetone (AT), and H_2O, and temperature profile for a feed of 1 mol % C_3H_6, 4 mol % O_2, and 95 mol % He at 250 °C.

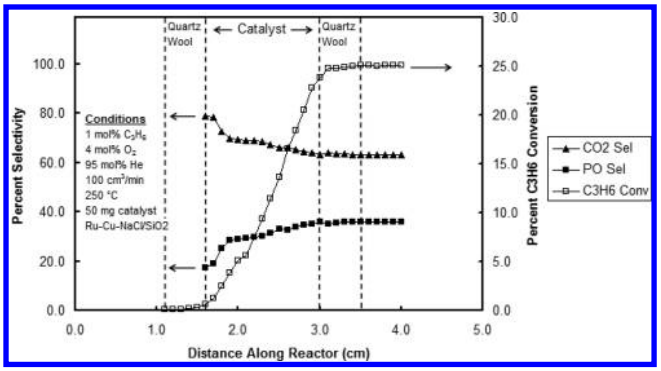

Figure 7. Propylene oxide (PO) selectivity, CO_2 selectivity, and propylene (C_3H_6) conversion profiles for a feed of 1 mol % C_3H_6, 4 mol % O_2, and 95 mol % He at 250 °C.

profiles for propylene conversion and PO and CO_2 selectivities are presented in Figure 7. The peak temperature was ~271 °C, a 21 °C temperature increase, where the peak is positioned at a distance of ~2.5 cm along the reactor (i.e., 1.0 cm within the catalyst bed). From Figure 6, peak PO, CO_2, and H_2O levels were 0.09%, 0.50%, and 0.63%, respectively. A comparison of these results to Figure 2 indicate that increasing O_2 increases the degree of propylene total combustion to CO_2, relative to epoxidation, which is an expected result. As seen in Figure 7, although propylene conversions increased and exhibited a peak level of ~25%, the maximum PO selectivity decreased to 38%, with CO_2 selectivity increasing to 62%. The PO selectivity also increased modestly with increasing residence time in the catalytic bed, in sharp contrast to the experiments at the O_2/C_3H_6 ratio of 2 (Figure 4). Significantly higher levels of AT and AC were also produced at the O_2/C_3H_6 ratio of 4, with peak concentrations of $\sim 0.3 \times 10^{-3}$ % and $\sim 0.2 \times 10^{-2}$ %, respectively. These levels are ~50% higher than those observed in Figure 2.

CONCLUSIONS

Detailed species concentration and temperature profiles have been obtained for the first time in a propylene epoxidation fixed-bed reactor packed with RuO_2−CuO−NaCl/SiO_2 catalysts. These profiles reveal significant new insights on the catalytic kinetics and mechanism of propylene epoxidation. In particular, spatial profiles indicate that acrolein (AC) formation was prompt and occurred early in the catalyst bed. In contrast, both acetone (AT) and propylene oxide (PO) production exhibited well-defined induction periods. These findings point to two different mechanisms associated with the formation of AC and AT/PO, respectively. The absence of any measurable propanal (PA) in the product mix also suggests that C2OMMP may be the preferred route for PO formation in this catalytic system. The spatial profiles reported represent information-rich data that are of significant utility for the development and validation of detailed chemical kinetic mechanisms for propylene partial oxidation in general and epoxidation in particular.

AUTHOR INFORMATION

Corresponding Author

*E-mail: ssenkan@gmail.com.

Notes

The authors declare no competing financial interest.

ACKNOWLEDGMENTS

We thank the Laboratory Catalyst Systems, LLC for providing access to their facilities, for the use of their catalytic materials discovery library and for financial support. B.Z. and D.N. acknowledge the support of the UCLA Graduate Division Fellowship and the NSF IGERT: Materials Creation Training Program (MCTP) (No. DGE-0654431) and the California NanoSystems Institute, respectively.

REFERENCES

(1) Cavani, F.; Teles, J. H. Sustainability in Catalytic Oxidation: An Alternative Approach or a Structural Evolution? *ChemSusChem* **2009**, *2*, 508−534.

(2) Nijhuis, T. A.; Makkee, M.; Moulijn, J. A.; Weckhuysen, B. M. Production of Propene Oxide: Catalytic Processes and Recent Developments. *Ind. Eng. Chem. Res.* **2006**, *45*, 3447−3459.

(3) Tullo, A. H.; Short, P. L. Propylene Oxide Routes Take Off. *Chem. Eng. News* **2006**, *84*, 22−23.

(4) Monnier, J. R. The direct epoxidation of higher olefins using molecular oxygen. *Appl. Catal., A* **2001**, *221*, 73−91.

(5) Vaughan, O. P. H.; Kyriakou, G.; Macleod, N.; Tikhov, M.; Lambert, R. M. Copper as a selective catalyst for the epoxidation of propene. *J. Catal.* **2005**, *236*, 401−404.

(6) Song, Z. X.; Mimura, N.; Bravo-Suarez, J. J.; Akita, T.; Tsubota, S.; Oyama, S. T. Gas-phase epoxidation of propylene through radicals generated by silica-supported molybdenum oxide. *Appl. Catal., A* **2007**, *316*, 142−151.

(7) Orzesek, H.; Schulz, R. P.; Dingerdissen, U.; Maier, W. F. Selective Oxidation of Propene with Air to Propylene Oxide, a Case Study of Autoxidation Versus Catalytic Oxidation with AMM-Catalysts. *Chem. Eng. Technol.* **1999**, *22*, 691−700.

(8) (a) Hayashi, T.; Han, L. B.; Tsubota, S.; Haruta, M. Formation of Propylene Oxide by the Gas-Phase Reaction of Propane and Propene Mixture with Oxygen. *Ind. Eng. Chem. Res.* **1995**, *34*, 2298−2304.

(b) Hayashi, T.; Tanaka, K.; Haruta, M. Selective Vapor-Phase Epoxidation of Propylene over Au/TiO_2 Catalysts in the Presence of Oxygen and Hydrogen. *J. Catal.* **1998**, *178*, 566−575. (c) Uphade, B. S.; Okumura, M.; Tsubota, S.; Haruta, M. Effect of physical mixing of CsCl with Au/Ti-MCM-41 on the gas-phase epoxidation of propene using H_2 and O_2: Drastic depression of H_2 consumption. *Appl. Catal., A* **2000**, *190*, 43−50. (d) Sinha, A. K.; Seelan, S.; Tsubota, S.; Haruta, M. A Three-Dimensional Mesoporous Titanosilicate Support for Gold Nanoparticles: Vapor-Phase Epoxidation of Propene with High Conversion. *Angew. Chem.* **2004**, *116*, 1572−1574;(e) *Angew. Chem., Int. Ed.* **2004**, *43*, 1546−1548.

(9) (a) Huang, J.; Akita, T.; Faye, J.; Fujitani, T.; Takei, T.; Haruta, M. Propene Epoxidation with Dioxygen Catalyzed by Gold Clusters. *Angew. Chem.* **2009**, *121*, 8002−8006;(b) *Angew. Chem., Int. Ed.* **2009**, *48*, 7862−7866.

(10) (a) Murata, K.; Kiyozumi, Y. Oxidation of propene by molecular oxygen over Ti-modified silicalite catalysts. *Chem. Commun.* **2001**, 1356−1357. (b) Murata, K.; Liu, Y.; Mimura, N.; Inaba, M. Direct vapor phase oxidation of propylene by molecular oxygen over MCM-41 or MCM-22 based catalysts. *Catal. Commun.* **2003**, *4*, 385−391.

(11) Berndt, T.; Brasel, S. Epoxidation of a Series of C_2−C_8 Olefins in the Gas Phase. *Chem. Eng. Technol.* **2009**, *32*, 1189−1194.

(12) Lei, Y.; Mehmood, F.; Lee, S.; Greeley, J.; Lee, B.; Seifert, S.; Winans, R. E.; Elam, J. W.; Meyer, R. J.; Redfern, P. C.; Teschner, D.; Schlogl, R.; Pellin, M. J.; Curtiss, L. A.; Vajda, S. Increased Silver Activity for Direct Propylene Epoxidation via Subnanometer Size Effects. *Science* **2010**, *328*, 224−228.

(13) Seubsai, A.; Kahn, S.; Senkan, S. New Catalytic Materials for the Direct Epoxidation of Propylene by Molecular Oxygen. *ChemCatChem* **2010**, *3*, 174−179.

(14) (a) Jankowiak, J. T.; Barteau, M. A. Ethylene epoxidation over silver and copper−silver bimetallic catalysts: I. Kinetics and selectivity. *J. Catal.* **2005**, *236*, 366−378. (b) Linic, S.; Piao, H.; Adib, K.; Barteau, M. A. Ethylene Epoxidation on Ag: Identification of the Crucial Surface Intermediate by Experimental and Theoretical Investigation of its Electronic Structure. *Angew. Chem., Int. Ed.* **2004**, *43*, 2918−2921.

(15) (a) Torres, D.; Lopez, N.; Illas, F.; Lambert, R. M. Low-Basicity Oxygen Atoms: A Key in the Search for Propylene Epoxidation Catalysts. *Angew. Chem.* **2007**, *119*, 2101−2104;(b) *Angew. Chem., Int. Ed.* **2007**, *46*, 2055−2058.

(16) Kulkarni, A.; Bedolla-Pantoia, M.; Singh, S.; Lobo, R. F.; Mavrikakis, M.; Barteau, M. A. Reactions of Propylene Oxide on Supported Silver Catalysts: Insights into Pathways Limiting Epoxidation Selectivity. *Top. Catal.* **2012**, *55*, 3−12.

(17) Senkan, S. Detailed Chemical Kinetic Modeling: Chemical Reaction Engineering of the Future. *Adv. Chem. Eng.* **1992**, *18*, 95−196.

(18) Wong, H.-W.; Cesa, M. C.; Golab, J. T.; Brazdil, J. F.; Green, W. H. Kinetic modeling to estimate fundamental yield bounds for selective propylene oxidation over bifunctional catalysts. *Appl. Catal., A* **2006**, *303*, 177−191.

(19) Fristrom, R. M.; Westenberg, A. A. *Flame Structure*; McGraw−Hill: New York, 1965; p 177.

(20) (a) Horn, R.; Williams, K. A.; Degenstein, N. J.; Schmidt, L. D. Syngas by catalytic partial oxidation of methane on rhodium: Mechanistic conclusions from spatially resolved measurements and numerical simulations. *J. Catal.* **2006**, *242*, 92−102. (b) Horn, R.; Korup, O.; Geske, M.; Zavyalova, U.; Oprea, I.; Schlogl, R. Reactor for in situ measurements of spatially resolved kinetic data in heterogeneous catalysis. *Rev. Sci. Instrum.* **2010**, *81*, 064102-1−064102-6.

(21) Zohour, B.; Noon, D.; Seubsai, A.; Senkan, S. New Insights on the Oxidative Coupling of Methane from Spatially Resolved Concentration and Temperature Profiles. *ChemCatChem.* **2013**, *5*, 2809−2812.

(22) Seubsai, A.; Senkan, S. The Effects of Cofeeding Chlorinated Hydrocarbons in the Direct Epoxidation of Propylene by Molecular Oxygen. *ChemCatChem* **2011**, *3*, 1751−1754.